Available online at www.sciencedirect.com
SCIENCE DIRECT®
International Journal of Solids and Structures 42 (2005) 5335–5355
INTERNATIONAL JOURNAL OF SOLIDS and STRUCTURES
www.elsevier.com/locate/ijsolstr

Shear banding analysis of geomaterials by strain gradient enhanced damage model

Jidong Zhao [a,*], Daichao Sheng [a], Weiyuan Zhou [b]

[a] School of Engineering, University of Newcastle, CALLAGHAN, NSW 2308, Australia
[b] Department of Hydraulic Engineering, Tsinghua University, 100084 Beijing, China

Received 12 July 2004; received in revised form 17 February 2005
Available online 28 March 2005

Abstract

Shear band localization is investigated by a strain-gradient-enhanced damage model for quasi-brittle geomaterials. This model introduces the strain gradients and their higher-order conjugate stresses into the framework of continuum damage mechanics. The influence of the strain gradients on the constitutive behaviour is taken into account through a generalized damage evolutionary law. A weak-form variational principle is employed to address the additional boundary conditions introduced by the incorporation of the strain gradients and the conjugate higher-order stresses. Damage localization under simple shear condition is analytically investigated by using the theory of discontinuous bifurcation and the concept of the second-order characteristic surface. Analytical solutions for the distributions of strain rates and strain gradient rates, as well as the band width of localised damage are found. Numerical analysis demonstrates the shear band width is proportionally related to the internal length scale through a coefficient function of Poisson's ratio and a parameter representing the shape of uniaxial stress–strain curve. It is also shown that the obtained distributions of strains and strain gradients are well in accordance with the underlying assumptions for the second-order discontinuous shear band boundary and the weak discontinuous bifurcation theory.

Keywords: Damage localization; Strain gradient plasticity; Discontinuous bifurcation; Second-order characteristic surface; Geomaterials

* Corresponding author. Tel.: +61 249215741; fax: +61 249216991.
E-mail addresses: jidong.zhao@newcastle.edu.au (J. Zhao), daichao.sheng@newcastle.edu.au (D. Sheng), zhouwy@tsinghua.edu.cn (W. Zhou).

0020-7683/$ - see front matter © 2005 Elsevier Ltd. All rights reserved.
doi:10.1016/j.ijsolstr.2005.02.029

1. Introduction

Shear band localization in geomaterials has attracted attention of many researchers over the last 30 years (see, e.g., Rudnicki, 1977; Pietruszczak and Mroz, 1981), and is generally treated as material instabilities by bifurcation theory (Hadamad, 1903; Hill, 1958; Thomas, 1961; Rudnicki and Rice, 1975; Ottosen and Runesson, 1991; De Borst and Van der Giessen, 1998). Substantive experimental data have proved that, during a typical localized failure process of a geomaterial, the underlying micro-scale mechanisms, such as crystal dislocation and development of defects and imperfections like pre-existing micro-crack and micro-void, may account for the irreversible deformation and stiffness degradation with damage accumulation in the material. These microscopic mechanisms also play a key role in triggering and forming shear band localization in the material, especially when the wavelength of deformation field is much larger than the dominant length scale of the microstructure. In such circumstances, the influence of the gradient terms of constitutive variables may be significant and can no longer be neglected. However, due to the absence of a length scale within the constitutive law and the neglect of these gradient terms, conventional continuum mechanics largely exhibits scale-independence when used to predict material behaviour. Width or spacing of shear band is generally unable to be determined. Moreover, in numerical simulation of localization, conventional continuum models may frequently encounter such problems as spurious mesh-dependency and high sensitivity to constitutive relations. To overcome the aforementioned difficulties, various approaches and models have been developed during the past decades, among which, higher-order gradient theories have recently revived much interest among scholars in both solid mechanics and materials science.

Gradient theories generally introduce local or non-local gradients of one or more field variables into the constitutive description of materials, and simultaneously one or more internal length scales into the governing equations. For example, Aifantis and his co-workers assumed the yielding stress is depend on the gradients of the plastic strain (Aifantis, 1984; Zbib and Aifantis, 1988, 1989, 1992), and based on this a series of similar models were developed to deal with problems such as stress singularity at dislocation lines and crack tips, shear band width and size effects (see, e.g., Triantafyllidis and Aifantis, 1986; Mühlhaus and Aifantis, 1991; De Borst and Mühlhaus, 1992; Gutkin and Aifantis, 1999). More recent development and review of this type gradient model may be referred to Tsagrakis and Aifantis (2002, 2003a,b), Konstantinidis and Aifantis (2002), Tsagrakis et al. (2003), Aifantis (2001, 2003). To discuss a variety of problems at small scale, Fleck and Hutchinson (1993, 1997) proposed a phenomenological higher-order theory by introducing higher-order stresses that are conjugate to the strain gradients into the constitutive relations, and later developed various mechanism-based strain gradient (MSG) plasticity theories (see, e.g., Gao et al., 1999; Fleck and Hutchinson, 2001). Some researchers also include damage mechanics into the gradient theory (see, e.g., Peerlings et al., 1996; Kuhl and Ramm, 2000; Zhou et al., 2002; Askes and Sluys, 2003).

While bifurcation theories within the framework of conventional continuum mechanics may be used to find the occurrence conditions for the inception of shear band localization, they are inadequate to describe the post-localization behaviours, as well as the microscopic effects on the macroscopic response. In this regard, gradient theories aforementioned exhibit an advantage due to the introduction of gradient terms and accordingly internal length scale limiters into the constitutive relations. By using gradient theories, various problems, such as the mesh dependency in numerical simulation of localization, and the size effects in meso- or micro-scale experiments, have been reasonably addressed. However, as much has been done on numerical simulation and experimental data calibration by gradient theories, little effort has been made on analytically investigating the formation of shear band localization, such as the band width and distributions of field variables within and outside the band. References addressing this subject are due to Aifantis (1984), Zbib and Aifantis (1988), Chambon et al. (1998, 2001) and Shi et al. (2000). Aifantis (1984, 1987), Zbib and Aifantis (1988) (see also other articles co-authored by Aifantis) linked the length scale coefficient in their gradient plasticity model with shear band width/spacing to interpret size effects typically exhibited in metals. Chambon et al. (1998, 2001) used a second grade model to address one-dimensional localization

problems in granular materials and implied a possible application to shear band analysis. Shi et al. (2000) used a micro-scale Taylor flow based MSG model to interpret shear band thickness in ductile materials. However, a direct and thorough investigation of shear band formation in geomaterials by gradient theories, which may reveal the distribution of all field variables in the deformation field as well as relate the band width with the internal length scale and other constitutive coefficients, is not yet available and thus needs to be addressed. This is the motivation of the paper.

In this paper, the problem of shear band localization is thoroughly investigated by a strain-gradient enhanced damage model previous proposed by the authors (2002). This model introduced damage mechanics to account for mechanical behaviours like irreversible deformation and stiffness degradation with damage accumulation in geomaterials. This model features of splitting the strain and strain gradients into elastic and inelastic part, which makes it essentially a derivative of the higher-order theory of Fleck and Hutchinson's (1997). Meanwhile, due to the inclusion of the strain gradients and their higher-order stress conjugates into the constitutive laws and governing equations, additional boundary conditions will be introduced and thus are addressed. In this regard, a weak-form variational formulation is developed to address the boundary restrictions for traction and higher-order traction in this paper. This formulation resembles those developed by Toupin (1962), Vardoulakis and Aifantis (1991) and Mühlhaus and Aifantis (1991), and is equivalent with the special case of second gradient theory of Germain's (1973) framework (also see Chambon et al., 1998, 2001).

In the following sections, the constitutive relations are reformulated within the framework of continuum damage mechanics based on the previous work of the authors (Zhou et al., 2002). In dealing with the damage localization, characteristic surfaces of second order (Thomas, 1961) are assumed to account for the continuity of velocities and their derivatives, and localized bands are formed by conjugated pairs of such surfaces. Typical hypothesis of weak discontinuous bifurcation is employed, which assumes that, inside the localized band, the material undergoes continuous damage loading, while outside the bands, the material undergoes elastic-damage unloading (see, e.g., Ottosen and Runesson, 1991). The formation of shear banding under simple shear condition is then analysed. Band widths in relation with these formations are found, and further discussions on boundary layer effects and size effect are carried out.

2. Constitutive description of the strain-gradient-enhance damage model

2.1. Strains and stresses in a higher-order continuum theory

In this paper, both strain and strain gradients are introduced in higher-order continuum theories (Toupin, 1962; Koiter, 1964; Mindlin, 1965; Fleck and Hutchinson, 1993, 1997). The symmetric strain tensor ε_{ij} and symmetric third-order strain gradient tensor η_{ijk} are assumed to be related to displacement u_i by the following expressions in a Cartesian coordinates system:

$$\begin{cases} \varepsilon_{ij} = \left(u_{i,j} + u_{j,i}\right)/2 \\ \eta_{ijk} = \left(u_{k,ij} + u_{k,ji}\right)/2 \end{cases} \tag{1}$$

It is further assumed that the rates of strains and strain gradients may be decomposed into elastic and damage parts respectively:

$$\begin{cases} \dot{\varepsilon}_{kl} = \dot{\varepsilon}^{\mathrm{e}}_{kl} + \dot{\varepsilon}^{\mathrm{d}}_{kl} \\ \dot{\eta}_{lmn} = \dot{\eta}^{\mathrm{e}}_{lmn} + \dot{\eta}^{\mathrm{d}}_{lmn} \end{cases} \tag{2}$$

Supposing the work-conjugates to ε_{ij} and η_{ijk} are denoted by the Cauchy stresses σ_{ij} and the higher-order stresses τ_{ijk}, respectively.

2.2. A variational formulation of the governing equations

Due to the introduction of the strain gradients and the higher-order stresses into the constitutive relations, additional boundary conditions will be needed in the model. Moreover, the equilibrium equations will also change upon the introduction of the gradient terms. A weak-form variational principle is used here to derive the equilibrium equations, following a similar approach used by Toupin (1962) for couple stress theory, Germain (1973) for the second grade theory, or Vardoulakis and Aifantis (1991) and Mühlhaus and Aifantis (1991) for their gradient plasticity models.

We first define the following equivalent stress rates according to (Mindlin, 1964, 1965; Toupin, 1962),

$$\dot{\Sigma}_{ij} = \dot{\sigma}_{ij} - \partial_k \dot{\tau}_{ijk} \tag{3}$$

where $\dot{\Sigma}_{ij}$ denotes the equivalent stress rates, $\dot{\sigma}_{ij}$ and $\dot{\tau}_{ijk}$ are the rates of the Cauchy stresses and the higher-order stresses, respectively. Note that the term $-\partial_k \dot{\tau}_{ijk}$ may be regarded as the eigen-stress tensor or the back-stress tensor according to Mindlin (1964).

According to the principle of virtual-work, the variation of the internal work is defined as

$$\delta W^{\text{int}} = \dot{\sigma}_{ij}\,\delta\dot{\varepsilon}_{ij} + \dot{\tau}_{ijk}\,\delta\dot{\eta}_{ijk} \tag{4}$$

Hence the following variation within a material volume V may be integrated by the local internal work over a representative volume V

$$\Delta W^{\text{int}} = \int_V \delta W^{\text{int}}\,\mathrm{d}V \tag{5}$$

The external surface S of V may be divided into two parts: one is the surface boundary S_Σ for static forces, and the other is S_u for dynamic forces. In classic continuum theories, these two boundaries are usually prescribed with tractions and velocities respectively. Due to the introduction of the strain gradients and the higher-order stress terms, extra conditions are required for the kinematic surface S_u. Generally, the velocity as well as its normal gradient along S_u should be initialized. This is equivalent to the following expression

$$\dot{u}_k = \dot{u}_k^0 \quad \text{and} \quad n_l \frac{\partial \dot{u}_k}{\partial x_l} = \dot{e}_k^0 \quad \text{on } S_u \tag{6}$$

where n_l is the norm of the surface S_u.

The virtual work done by external force, ΔW^{ext}, includes contributions from the surface tractions, higher-order tractions, body forces and inertial forces. An inertial force can be treated as a negative body force and its work is the product of the material density and the second-order differentials, i.e., $-\rho D^t \dot{u}_i$, with $D^t = \partial_t + \dot{u}_j \partial_j$ denoting the material differential. In the following formulations, the flux term in the material differential will be neglected. Hence the material differential may be replaced by the time partial–differential. The work done by external forces is thus:

$$\Delta W^{\text{ext}} = \int_V \left(\dot{f}_i - \rho D^t \dot{u}_i\right) \delta u_i\,\mathrm{d}V + \int_S \left(\dot{t}_i\,\delta u_i + \dot{r}_i n_k \partial_k\,\delta u_i\right)\mathrm{d}S \tag{7}$$

where $\dot{f}_i$ is the body force, $\dot{t}_i$ and $\dot{r}_i$ are the rates of the traction and the higher-order traction force, respectively, and they are related to the Cauchy stresses and the higher-order stresses.

According to the principle of virtual work, the following equation holds:

$$\Delta W^{\text{int}} = \Delta W^{\text{ext}} \tag{8}$$

Substitution of (4), (5) and (7) into (8) leads to

$$\int_V \left\{\dot{\sigma}_{ij}\,\delta\dot{\varepsilon}_{ij} + \dot{\tau}_{ijk}\,\delta\dot{\eta}_{ijk} - \left(\dot{f}_i - \rho D^t \dot{u}_i\right)\delta u_i\right\}\mathrm{d}V = \int_S \left(\dot{t}_i\,\delta u_i + \dot{r}_i n_k \partial_k\,\delta u_i\right)\mathrm{d}S \tag{9}$$

To compute the surface integral of the right-hand-side term of Eq. (9), the virtual velocity and its normal gradients must vanish on S_u:

$$\delta\dot{u}_k = 0 \quad \text{and} \quad n_l \frac{\partial\, \delta\dot{u}_k}{\partial x_l} = 0 \quad \text{on } S_u \tag{10}$$

In order to derive the equilibrium equations and the corresponding boundary conditions from (9), the internal work presented in (4) is re-written in the following form

$$\Delta W^{\text{int}} = \partial_i\left[\left(\dot{\sigma}_{ij} - \partial_k \dot{\tau}_{ijk}\right)\delta u_j\right] - \partial_i\left(\dot{\sigma}_{ij} - \partial_k \dot{\tau}_{ijk}\right)\delta u_j + \partial_k\left(\dot{\tau}_{ijk}\partial_i\, \delta u_j\right) \tag{11}$$

From the divergence theorem we have

$$\Delta W^{\text{int}} = \int_S n_i\left(\dot{\sigma}_{ij} - \partial_k \dot{\tau}_{ijk}\right)\delta u_j \,\mathrm{d}S - \int_V \partial_i\left(\dot{\sigma}_{ij} - \partial_k \dot{\tau}_{ijk}\right)\delta u_j \,\mathrm{d}V + \int_S n_k\left(\dot{\tau}_{ijk}\partial_i\, \delta u_j\right)\mathrm{d}S \tag{12}$$

Therefore, Eq. (9) becomes

$$\begin{aligned}&\int_S n_i\left(\dot{\sigma}_{ij} - \partial_k \dot{\tau}_{ijk}\right)\delta u_j \,\mathrm{d}S - \int_V \partial_i\left(\dot{\sigma}_{ij} - \partial_k \dot{\tau}_{ijk}\right)\delta u_j \,\mathrm{d}V + \int_S n_k\left(\dot{\tau}_{ijk}\partial_i\, \delta u_j\right)\mathrm{d}S \\ &\quad = \int_V \left(\dot{f}_i - \rho D^t \dot{u}_i\right)\delta u_i \,\mathrm{d}V + \int_S \left(\dot{t}_i\, \delta u_i + \dot{r}_i n_k \partial_k\, \delta u_i\right)\mathrm{d}S\end{aligned} \tag{13}$$

The equilibrium equation is obtained by the volume integral in Eq. (13)

$$\partial_i\left(\dot{\sigma}_{ij} - \partial_k \dot{\tau}_{ijk}\right) + \dot{f}_j = \rho D^t \dot{u}_j \tag{14}$$

The equilibrium equation may also be expressed in the form of equivalent stresses

$$\partial_i \dot{\Sigma}_{ij} + \dot{f}_j = \rho D^t \dot{u}_j \tag{15}$$

If all the terms in (14) are time-independent, the right-hand side will become zero. Hence the static equilibrium equation is obtained

$$\sigma_{ij,i} - \tau_{ijk,ik} + f_j = 0 \quad \text{or} \quad \partial_i \dot{\Sigma}_{ij} + \dot{f}_j = 0 \tag{16}$$

Note that the surface integrals in Eq. (9) include not only δu_i but also its gradients. In order to derive the static boundary conditions from the surface integrals, the following integral is considered

$$I = \int_S n_k\left(\dot{\tau}_{ijk}\partial_i\, \delta u_j\right)\mathrm{d}S \tag{17}$$

$\partial_i\, \delta u_j$ is decomposed into normal and tangential parts:

$$\partial_i\, \delta u_j = n_i n_k \partial_k\, \delta u_j + (\delta_{ik} - n_i n_k)\partial_k\, \delta u_j \tag{18}$$

If the following symbols are adopted

$$D = n_k \partial_k, \quad D_i = (\delta_{ik} - n_i n_k)\partial_k \tag{19}$$

with D denoting the normal differential where the normal vector is n_k in local coordinate system, and D_i being the surface gradient operator.

From Eqs. (17)–(19), we have

$$n_k \dot{\tau}_{ijk}\partial_i\, \delta u_j = n_k \dot{\tau}_{ijk} D_i\, \delta u_j + n_k \dot{\tau}_{ijk} n_i D\, \delta u_j \tag{20}$$

The first term on the right-hand side of the above equation may be transformed into

$$n_k \dot{\tau}_{ijk} D_i\, \delta u_j = D_i\left(n_k \dot{\tau}_{ijk}\, \delta u_j\right) - n_k D_i \dot{\tau}_{ijk}\, \delta u_j - (D_i n_k)\dot{\tau}_{ijk}\, \delta u_j \tag{21}$$

In order to calculate the first term of the right-hand side of Eq. (21), the following operator is adopted:

$$D_j F_j = D_k n_k n_j F_j - n_q e_{qpm} \partial_p (e_{mkj} n_k F_j) \tag{22}$$

here e_{ijk} is the permutation tensor. We further assume

$$A_m = e_{mkj} n_k F_j, \quad F_j = n_k \dot{\tau}_{ijk}\, \delta u_i \tag{23}$$

Then the following form integral must be zero on a closed surface

$$\int_S e_{qpm} \partial_p A_m n_q \, \mathrm{d}S = 0 \tag{24}$$

As it also holds

$$n_j \partial_k \dot{\tau}_{ijk} = n_j D_k \dot{\tau}_{ijk} + n_k n_j D \dot{\tau}_{ijk} \tag{25}$$

Extraction of all the surface integrals in (13) leads to

$$\begin{aligned} &\int_S \left[n_j \dot{\sigma}_{jk} - n_i n_j D \dot{\tau}_{ijk} - (n_i D_j + n_j D_i) \dot{\tau}_{ijk} + (n_i n_j D_l n_l - D_j n_i) \dot{\tau}_{ijk} \right] \delta u_k \, \mathrm{d}S + \int_S n_i n_j \dot{\tau}_{ijk} D\, \delta u_k \, \mathrm{d}S \\ &\quad = \int_S \dot{t}_k \, \delta u_k \, \mathrm{d}S + \int_S \dot{r}_k D\, \delta u_k \, \mathrm{d}S \end{aligned} \tag{26}$$

Hence the rate forms of the boundary traction and the higher-order external force (or double surface traction in term of Germain (1973)) may be obtained

$$\dot{t}_k = n_j \dot{\sigma}_{jk} - n_i n_j D \dot{\tau}_{ijk} - (n_i D_j + n_j D_i) \dot{\tau}_{ijk} + (n_i n_j D_l n_l - D_j n_i) \dot{\tau}_{ijk} \tag{27}$$

$$\dot{r}_k = n_i n_j \dot{\tau}_{ijk} \tag{28}$$

The boundary traction conditions in (27) may be further simplified as

$$\dot{t}_k = n_i \left(\dot{\sigma}_{ik} - \partial_j \dot{\tau}_{ijk} \right) - D_j (n_i \dot{\tau}_{ijk}) + n_i n_j (D_l n_l) \dot{\tau}_{ijk} \tag{29}$$

Note that the above attained results largely resemble those obtained by Germain (1973) for the special case of second gradient theory. The only difference between them is, the intrinsic stress defined in Eq. (68) of Germain (1973) involves a term for long range volumetric double force, while the equivalent stress defined in Eq. (3) of this paper does not consider this term. Form most boundary/initial value problems, it is always difficult to specify this term, while neglect of it generally has litter effect on the solutions.

2.3. Reformulation of the strain-gradient-enhanced damage model

To simplify the presentation, the isotropic and anisotropic strain-gradient-enhanced (SGE) damage models by Zhou et al. (2002) are generalized into a united formulation in this section. The following expressions for the rate of the Cauchy stresses and the higher-order stresses are adopted:

$$\begin{cases} \dot{\sigma}_{ij} = D_{ijkl} \left(\dot{\varepsilon}_{kl} - \dot{\varepsilon}^{\mathrm{d}}_{kl} \right) \\ \dot{\tau}_{ijk} = l^2 D_{ijkl} \delta_{mn} \left(\dot{\eta}_{lmn} - \dot{\eta}^{\mathrm{d}}_{lmn} \right) \end{cases} \tag{30}$$

where D_{ijkl} denotes the elasto-damage stiffness tensor of the material, which may accounts for the degradation due to accumulation of damage, δ is the second-order Kronecker delta, and l represents a material length scale which reflects the influence of crystal or grain size and microstructures, such as micro-void and micro-cracks in geomaterials, on the macroscopic mechanical response. Note that the expressions in Eq. (30) are not the only choice. The formulation adopted here is based on a similar concept that was used by Shu and Fleck (1999), who expressed the constitutive relations by the macroscopic average of the micro-

scale mechanical behaviors and, related the higher-order stress to the local average variation of Cauchy stress on the micro-scale, e.g., $\dot{\tau}_{ijk} = l^2\partial\dot{\sigma}_{ij}/\partial x_k$. Consequently, the abovementioned formulation may be generalized into a more general constitutive relations proposed by Mindlin (1964) and/or Fleck and Hutchinson (1997), if taking no account of damage. While the initially phenomenological Fleck–Hutchinson theory is intended to model metal plasticity, such appropriate changes as stated above, make it still suitable to describe mechanical behavior of geomaterials. In fact, as has been stated by Chambon et al. (2001), various features of geomaterials make phenomenological theories the only possible way of study.

A damage flow rule usually takes the same form as that in classic plasticity theory:

$$\dot{\varepsilon}^{\mathrm{d}}_{kl} = \dot{\lambda}\frac{\partial g}{\partial \sigma_{kl}}, \quad \dot{\eta}^{\mathrm{d}}_{lmn} = \dot{\lambda}\frac{\partial g}{\partial \tau_{lmn}}, \quad \dot{\Theta} = \dot{\lambda}\frac{\partial g}{\partial Q} \tag{31}$$

where $\dot{\lambda}$ is the rate of damage multiplier, $g = g(\Theta, Q, \kappa)$ denotes a damage potential in the composite stress space constituted by the Cauchy stresses and the higher-order stresses, κ denotes an internal variable related with dissipation processes, Θ and Q are generalized damage variable and its thermodynamic conjugate force respectively and they are used for both isotropic and anisotropic damage. In this paper the dissipation rate of κ is assumed to be equal to $\dot{\lambda}$, i.e. $\dot{\kappa} = \dot{\lambda}$ (similarly, see, e.g., Kuhl and Ramm, 2000). In the case of isotropic damage, Θ and Q are scalars, whereas for anisotropic damage, they are second-order tensors:

$$\Theta = \begin{cases} d \\ \Omega_{ij} \end{cases}, \quad Q = \begin{cases} Y, & \text{isotropic damage case,} \\ Y_{ij}, & \text{anisotropic damage case,} \end{cases} \tag{32}$$

where d and Ω_{ij} denote isotropic scalar damage variable and the second-order fabric damage tensor, respectively, Y and Y_{ij} are the thermodynamic conjugates to the scalar d and the anisotropic damage tensor Ω_{ij}, respectively. Their detailed expressions are referred to Eq. (5) and (23) in Zhou et al. (2002).

Supposing that the damage yield function has the following expression

$$f = f\left(\sigma_{ij}, \tau_{ijk}, \Theta, \kappa\right) \tag{33}$$

the consistency condition of the damage surface leads to the following equation:

$$\dot{f} = \frac{\partial f}{\partial \sigma_{ij}}\dot{\sigma}_{ij} + \frac{\partial f}{\partial \tau_{lmn}}\dot{\tau}_{lmn} + \frac{\partial f}{\partial \Theta}\dot{\Theta} + \frac{\partial f}{\partial \kappa}\dot{\kappa} = 0 \tag{34}$$

Substituting Eq. (31) into (34) leads to

$$\frac{\partial f}{\partial \sigma_{ij}}\dot{\sigma}_{ij} + \frac{\partial f}{\partial \tau_{lmn}}\dot{\tau}_{lmn} - \dot{\gamma}H = 0 \tag{35}$$

where

$$H = -\left(\frac{\partial f}{\partial \Theta}\frac{\partial g}{\partial Q} + \frac{\partial f}{\partial \kappa}\right) \tag{36}$$

Hereafter H is referred to as the hardening/softening modulus for the strain-gradient-enhanced (SGE) damage model, which is analogue to that in the classic plasticity theory.

Manipulation of Eqs. (2), (30), (35) and (36) can result in the following expression for the damage multiplier:

$$\dot{\gamma} = \left(\frac{\partial f}{\partial \sigma_{ij}}D_{ijab}\dot{\varepsilon}_{ab} + \frac{\partial f}{\partial \tau_{xyp}}l^2 D_{xylm}\delta_{pn}\dot{\eta}_{lmn}\right)\Big/ A \tag{37}$$

where

$$A = H + \frac{\partial f}{\partial \sigma_{ab}}D_{abcd}\frac{\partial g}{\partial \sigma_{cd}} + \frac{\partial f}{\partial \tau_{uvw}}l^2 D_{uvxy}\delta_{wz}\frac{\partial g}{\partial \tau_{xyz}} \tag{38}$$

Generalization of Eqs. (2), (30), (31), (37) and (38) leads to the following incremental constitutive relations for the SGE damage model:

$$\begin{cases} \dot{\sigma}_{ij} = \left(D_{ijkl} - \dfrac{1}{A} D_{ijab} \dfrac{\partial g}{\partial \sigma_{ab}} \dfrac{\partial f}{\partial \sigma_{cd}} D_{cdkl} \right) \dot{\varepsilon}_{kl} - \dfrac{1}{A} D_{ijpq} \dfrac{\partial g}{\partial \sigma_{pq}} \dfrac{\partial f}{\partial \tau_{rst}} l^2 D_{rsuv} \delta_{tw} \dot{\eta}_{uvw} \\ \dot{\tau}_{ijk} = \left(D_{ijlm} \delta_{kn} - \dfrac{1}{A} l^2 D_{ijab} \delta_{kc} \dfrac{\partial g}{\partial \tau_{abc}} \dfrac{\partial f}{\partial \tau_{xyp}} D_{xylm} \delta_{pn} \right) l^2 \dot{\eta}_{lmn} - \dfrac{1}{A} l^2 D_{ijqr} \delta_{ks} \dfrac{\partial g}{\partial \tau_{qrs}} \dfrac{\partial f}{\partial \sigma_{uv}} D_{uvwt} \dot{\varepsilon}_{wt} \end{cases} \tag{39}$$

Eq. (39) presents a form of coupled strains and strain gradients for both the Cauchy stresses and the higher-order stresses. As can be seen, the Cauchy stress increments do not only depend on the strain increments, but also on the strain gradient increments. The same applies to the higher-order stress increments. We see that the introduction of the strain gradients and their conjugate higher-order stresses into the constitutive relations changes the normal structure of classic elastoplastic models.

3. Shear banding analysis of damage localization

In this section, shear banding localization for simple shear tests will be investigated using the model present above and discontinuous bifurcation theory. In literature, the shear banding problem has long been treated by gradient theories for times. For example, Aifantis (1984) has derived a shear band solution that provides the width of the localized deformation zone. Chambon et al. (1998) have also developed analytical solutions of boundary value problems by second grade generalization of a common softening model to verify the numerical simulations of localization of one dimensional bar. They further implied potential applications of this model to the study of a wide range of localization phenomena and/or boundary layer effects for both granular materials and cohesive geomaterials (Chambon et al., 2001).

The following assumptions are made in the analysis:

(1) Second-order discontinuous surfaces. Here in this paper, the discontinuous surfaces that bound the shear band with the rest area is supposed to be a second-order one defined by Thomas (1961), which is characterized by the continuity of the displacement and its gradient along the normal direction of the characteristic surface, while the second-order gradient of the displacement exhibiting a jump across the surface.

(2) Stress–strain relations. We further assume the constitutive cones on both sides of the surface are characterized by the strain-gradient-enhanced damage model formulated above. For the sake of simplicity, only isotropic damage is considered. Bi-linear uniaxial stress–strain relations are assumed in the following analysis of plane shearing of geomaterials (Fig. 1), which share a similarity of those adopted by Chambon et al. (1998). Assume the uniaxial tensile strength is σ_u, the elastic modulus is E, and the bulk modulus is K and the shear modulus is G. The following evolutionary law is adopted for the isotropic damage

$$d(\kappa) = \begin{cases} \dfrac{\kappa_c}{\kappa} \dfrac{\kappa - \kappa_0}{\kappa_c - \kappa_0}, & \text{if } \kappa_0 < \kappa \leqslant \kappa_c \\ 1, & \text{if } \kappa_c < \kappa \end{cases} \tag{40}$$

The internal variable κ is assumed to be equal to the following equivalent strain ε:

$$\kappa = \varepsilon = \sqrt{\frac{2}{3} \varepsilon_{ij} \varepsilon_{ij}} \tag{41}$$

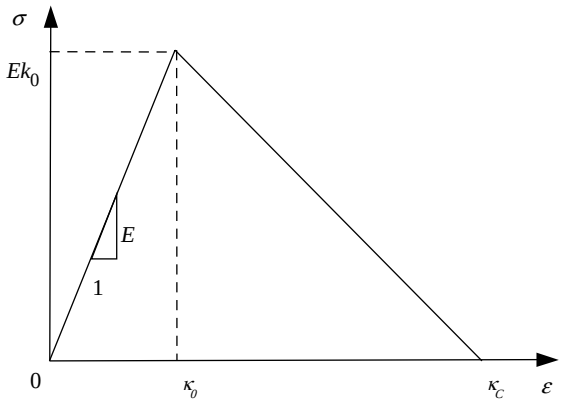

Fig. 1. Bi-linear stress–strain relation.

Thus the following bi-linear uniaxial stress-strain relations (as depicted in Fig. 1) may be obtained

$$\sigma = \begin{cases} E\varepsilon, & \text{if } \varepsilon < \kappa_0 \\ \dfrac{\kappa_0}{\kappa}\dfrac{\kappa_c - \kappa}{\kappa_c - \kappa_0} E\varepsilon, & \text{if } \kappa_0 \leqslant \varepsilon < \kappa_c \\ 0, & \text{if } \varepsilon \geqslant \kappa_c \end{cases} \tag{42}$$

(3) Shear band formation. The plane pure shear test and formation of the shear band localization are illustrated in Fig. 2. The band width is assumed to be h. The coordinate system is such chosen that axis y is perpendicular to the shear direction, while axis x parallel with the shear direction. The origin of the coordinate is located at the symmetric centre of the band. Due to the symmetry, only the upper half plane ($y \geqslant 0$) is considered.

(4) Boundary conditions. The shear band is assumed to be located in an infinite domain imposed by only shear stress at the infinite far boundary. This implies, only remote shear traction force is considered, while the double traction force (or alternatively higher-order traction) at this boundary is neglected.

(5) Discontinuous bifurcation. It is further assumed before the inception of localization bifurcation, the deformation in the material is homogeneous. Once κ reaches its critical value κ_0, the initial bifurcation state is attained. And a weak form discontinuous bifurcation according to the bifurcation theory will

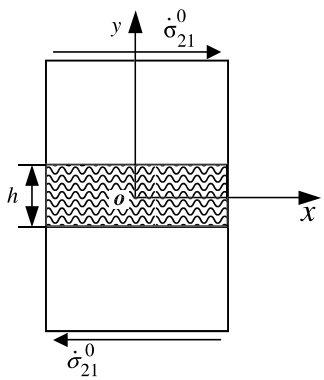

Fig. 2. Simple shear test and shear banding.

occur afterwards. That is, damage loading dominates the mechanical behaviors within the band during shear band localization, while elasto-damage unloading prevails outside the band.

Some remarks should be addressed here on the physical interpretation of the softening laws in Eq. (42). As it is assumed here the internal variable κ is directly related with the total strain in Eq. (41), the progressive deformation in the material will induce an accumulation of κ. When the magnitude of κ is lower that its lower threshold κ_0, damage process is assumed not to happen and the first order stress–strain relation is therefore elastic. However, when it is large enough to reach κ_0, irreversible damage will be triggered according to Eq. (40). At this point, several types of laws may be assumed further, say, hardening, perfectly damaging and softening ones (as see the patch conditions in Chambon et al. (1998)). Here we adopt the last type, which implies once the material reaches its peak stress through elastic response, further loading will result in a softening(/damaging) branch, while unloading along a reverse line of the previous elastic branch. In connection with the assumption for discontinuous bifurcation in (5), the damage loading within the band is clearly controlled by the softening branch, while outside the band the elastic–damage unloading evolves along the reverse elastic branch. It will be shown that these assumptions combined together make it possible to reach an analytical solution for the particular pure shear problem.

Let us continue with simple shear test. It is clear the displacement is horizontal, i.e. $u = u_x \neq 0$, and is only related to y. If $\gamma = \mathrm{d}u/\mathrm{d}y$ is the engineering shear strain, non-zero strain and strain gradient may be written as

$$\begin{cases} \varepsilon_{12} = \varepsilon_{21} = \dfrac{1}{2}\dfrac{\partial u}{\partial y} = \dfrac{1}{2}\gamma \\ \eta_{221} = \dfrac{\mathrm{d}^2 u}{\mathrm{d}y^2} = \gamma_{,2} \end{cases} \tag{43}$$

We also assume that the shear strain γ is continuous throughout the material and monotonically varies from its maximum at the centre to an imposed value at far field. In the upper half space we thus have

$$\gamma > 0, \quad \gamma_{,2} < 0 \tag{44}$$

The following equivalent strain and equivalent strain gradient are then obtained

$$\varepsilon = \frac{\gamma}{\sqrt{3}}, \quad \eta = \sqrt{\frac{1}{4}\eta_{ijk}\eta_{ijk}} = -\frac{1}{2}\gamma_{,2} \tag{45}$$

The equilibrium equation (16) without body force becomes

$$\sigma_{21,2} - \tau_{221,22} = 0 \tag{46}$$

Integration of the above equation along the y direction leads to

$$\sigma_{21} - \tau_{221,2} = \sigma_{21}^0 \tag{47}$$

The rate form of the this equation is

$$\dot{\sigma}_{21} - \dot{\tau}_{221,2} = \dot{\sigma}_{21}^0 \tag{48}$$

From the constitutive equation (39), we obtain the following stress and higher-order stress for the damage flow stage:

$$\begin{cases} \sigma_{21} = \dfrac{\kappa_0}{\kappa}\dfrac{\kappa_c - \kappa}{\kappa_c - \kappa_0} G\varepsilon_{21} = \dfrac{\kappa_0 G}{2}\dfrac{\left(\sqrt{3}\kappa_c - \gamma\right)}{\kappa_c - \kappa_0} \\ \tau_{221} = l^2 \dfrac{\kappa_0}{\kappa}\dfrac{\kappa_c - \kappa}{\kappa_c - \kappa_0}\left(K + \dfrac{4}{3}G\right)\eta_{221} = l^2 \dfrac{\kappa_0}{\kappa}\dfrac{\kappa_c - \kappa}{\kappa_c - \kappa_0}\left(K + \dfrac{4}{3}G\right)\gamma_{,2} \end{cases} \tag{49}$$

It is reasonable to assume that before the inception of localization bifurcation, the deformation in the material is homogeneous. Once the damage is accumulated so that κ reaches its critical value κ_0, the initial bifurcation state is attained. At this time, the higher-order stress rate is approximated as follows

$$\dot{\tau}_{221} = l^2\left(K + \frac{4}{3}G\right)\dot{\gamma}_{,2} \tag{50}$$

The Cauchy stress rate is then

$$\begin{cases} \dot{\sigma}_{21} = -\dfrac{\kappa_0 G}{2(\kappa_c - \kappa_0)}\dot{\gamma}, & \text{if } \dot{\gamma} \geqslant 0 \\ \dot{\sigma}_{21} = \dfrac{G}{2}\dot{\gamma}, & \text{if } \dot{\gamma} < 0 \end{cases} \tag{51}$$

Shear band localization is generally treated as a weak discontinuous bifurcation. According to the bifurcation theory, damage loading dominates the mechanical behaviors within the band during shear band localization, and elasto-damage unloading prevails outside the band. Thus, from the above equation we have

$$\begin{cases} -\dfrac{\kappa_0 G}{2(\kappa_c - \kappa_0)}\dot{\gamma} - l^2\left(K + \dfrac{4}{3}G\right)\dot{\gamma}_{,22} = \tau^0, & \dot{\gamma} \geqslant 0,\ 0 \leqslant y \leqslant \dfrac{h}{2} \\ \dfrac{G}{2}\dot{\gamma} - l^2\left(K + \dfrac{4}{3}G\right)\dot{\gamma}_{,22} = \tau^0, & \dot{\gamma} < 0,\ \dfrac{h}{2} < y \leqslant \infty \end{cases} \tag{52}$$

The general solution to the above differential equation is

$$\begin{cases} \dot{\gamma} = -\dfrac{2(\kappa_c - \kappa_0)\dot{\sigma}^0_{21}}{\kappa_0 G} + C_1 \cos\sqrt{\dfrac{3\kappa_0 G}{2l^2(\kappa_c - \kappa_0)(3K + 4G)}}y + C_2 \sin\sqrt{\dfrac{3\kappa_0 G}{2l^2(\kappa_c - \kappa_0)(3K + 4G)}}y, & 0 \leqslant y \leqslant \dfrac{h}{2} \\ \dot{\gamma} = \dfrac{2\dot{\sigma}^0_{21}}{G} + C_3 e^{-\sqrt{\dfrac{G}{2l^2(3K + 4G)}}y}, & \dfrac{h}{2} < y \leqslant \infty \end{cases} \tag{53}$$

where h is the band width to be determined. Unknown parameters C_i ($i = 1,2,3$) may be determined by the following boundary conditions:

(1) Anti-symmetry of the shear strain rate under pure shear conditions

$$\dot{\gamma}_{,2}|_{y=0} = 0 \tag{54}$$

(2) Continuity of the displacement rate and its first derivative along the normal direction of the band for the second-order discontinuous surface of Thomas (1961)

$$[\dot{\gamma}]|_{y=h/2} = \dot{\gamma}|_{y=(h/2)^+} - \dot{\gamma}|_{y=(h/2)^-} = 0 \tag{55}$$

$$[\dot{\gamma}_{,2}]|_{y=h/2} = \dot{\gamma}_{,2}|_{y=(h/2)^+} - \dot{\gamma}_{,2}|_{y=(h/2)^-} = 0 \tag{56}$$

(3) Damage loading within the band requires $\dot{\gamma} \geqslant 0$, while elasto-damage unloading outside the band requires $\dot{\gamma} \leqslant 0$. Therefore at the boundary it is required $\dot{\gamma} = 0$. That is

$$\dot{\gamma}|_{y=(h/2)^+} = \dot{\gamma}|_{y=(h/2)^-} = 0 \tag{57}$$

Noted that the third condition is exactly equivalent to the soft piece of the patch conditions in Chambon et al. (1998). Upon collection of the above four equations, the parameters $C_i\,(i=1,2,3,4)$ can thus be determined. After some manipulation, the following expressions for the shear strain rate may be attained

$$\begin{cases} \dot{\gamma} = \dfrac{2\dot{\sigma}^0_{21}}{G}\left(1-\chi+\dfrac{\beta\chi\cos(\xi y)}{\beta\cos(\xi h/2)-\xi\sin(\xi h/2)}\right), & 0\leqslant y\leqslant \dfrac{h}{2} \\ \dot{\gamma} = \dfrac{2\dot{\sigma}^0_{21}}{G}\left(1+\dfrac{\chi\xi\sin(\xi h/2)}{\beta\cos(\xi h/2)-\xi\sin(\xi h/2)}e^{\beta\left(\frac{h}{2}-y\right)}\right), & \dfrac{h}{2}< y\leqslant\infty \end{cases} \tag{58}$$

where

$$\chi=\frac{\kappa_c}{\kappa_0},\quad \xi=\sqrt{\frac{3}{2l^2(\chi-1)(3K/G+4)}},\quad \beta=\sqrt{\frac{1}{2l^2(3K/G+4)}}. \tag{59}$$

χ is a coefficient representing the shape of the uniaxial stress–strain curve.

The rates of the shear strain gradient inside and outside the shear band can then be readily obtained from (58) as:

$$\begin{cases} \dot{\gamma}_{,2} = -\dfrac{2\dot{\sigma}^0_{21}}{G}\left(\dfrac{\beta\chi\xi\sin(\xi y)}{\beta\cos(\xi h/2)-\xi\sin(\xi h/2)}\right), & 0\leqslant y\leqslant \dfrac{h}{2} \\ \dot{\gamma}_{,2} = -\dfrac{2\dot{\sigma}^0_{21}}{G}\left(\dfrac{\chi\beta\xi\sin(\xi h/2)}{\beta\cos(\xi h/2)-\xi\sin(\xi h/2)}e^{\beta\left(\frac{h}{2}-y\right)}\right), & \dfrac{h}{2}< y\leqslant\infty \end{cases} \tag{60}$$

The band width can then be obtained from Eqs. (57) and (58)

$$h=\frac{2}{\xi}\left(k\pi-\arctan\left(\frac{\beta}{\xi(\chi-1)}\right)\right) \tag{61}$$

where $k=1,2,\ldots$ denote the wave number. As the shear band localization belongs to the case of short wavelength, we take $k=1$. Therefore, the shear band width has the following expression:

$$h=\frac{2}{\xi}\left(\pi-\arctan\left(\frac{\beta}{\xi(\chi-1)}\right)\right) \tag{62}$$

Supposing that the following relation between the bulk modulus and the shear modulus holds

$$\frac{K}{G}=\frac{2(1+v)}{3(1-2v)} \tag{63}$$

with v being Poisson's ratio, the parameters ξ and β are then given as:

$$\xi=\frac{1}{2l}\sqrt{\frac{(1-2v)}{(\chi-1)(1-v)}},\quad \beta=\frac{1}{2l}\sqrt{\frac{(1-2v)}{3(1-v)}} \tag{64}$$

Therefore, the shear band width can now be expressed as a function of v, χ and the internal length scale l

$$h=\varpi l\quad \text{or alternatively}\quad \frac{h}{l}=\varpi \tag{65}$$

where

$$\varpi=4\sqrt{\frac{(\chi-1)(1-v)}{(1-2v)}}\left(\pi-\arctan\left(\frac{1}{\sqrt{3(\chi-1)}}\right)\right) \tag{66}$$

A note should be made that in Chambon et al. (2001), a local elasto-plastic second gradient model has been applied to the analysis of plain strain shear band and an analytical method has been developed to find the solutions. As has been stated in their conclusion, such a method may be possibly used to achieve analytical solutions for all microstructured models and even further, within the damage mechanics framework. Here the method treating the simple shearing problem in this paper though not necessarily the same, may partially serve as a good proof of their conclusion. Nevertheless, the significance of obtaining analytical solutions to some boundary value problems should again be emphasized since these solutions may be used as benchmarks for numerical simulations. Moreover, by the solution in this paper, the internal length scale in the SGE damage model is directly link with the shear band width, which provides a possible approach to calibrate it by experiments.

4. Numerical analysis and discussions

4.1. Internal length scale and shear band width

From Eq. (64) we find, under the current assumptions of constitutive relations and simple plane shear conditions, the shear band width is proportional to the internal length scale. The proportionality is a material parameter ϖ, which is controlled by Poisson's ratio v and the coefficient χ for the shape of the uniaxial stress–strain curve. To further illustrate the influence of v and χ on the width, numerical investigations are carried out and the results are presented in Fig. 3. In the figure, the band width is normalized by the internal length scale l, and v and χ are confined to the follow range:

$$v \in [0.0, 0.5], \quad \chi \in [1, +\infty] \tag{67}$$

As can be seen, larger values for v and χ generally result in larger shear band width. The band width is also more sensitive to χ than to v. When $\chi = 1.0$, which implies $\kappa_c = \kappa_0$ and there is no softening period in the uniaxial stress–strain relation, the material exhibits a typical elasto-brittle feature (as is shown in Fig. 4). The shear bands for this kind of materials are typically clear-cut shear cracks and hence may be regarded to have a zero band width, which is in accordance with the results in Fig. 3a. This extreme case of localization may be categorized as the strong discontinuous bifurcation. On the other hand, when $\chi \to +\infty$, the band width approaches infinite (Fig. 3a). In this case, the uniaxial stress–strain curve displays a characteristic of elasto-perfect-damage material (analogue to elastic perfectly plastic, as shown in Fig. 4). For this kind of material, once the damage reaches the critical magnitude, infinite damage flow will occur in the material. In this case, a long wavelength limit applies and no obvious shear band may be observed.

Fig. 3b shows that the band width remains more or less steady when Poisson's ratio is smaller than 0.4. When the Poisson's ratio approaches 0.5, the band width increases dramatically, and when $v = 0.5$, the band width approaches the infinite. In fact, materials with a small value of v typically demonstrate the characteristic of solid. In this case, the formation of shear band will be constrained by adjacent layers and thus the band width will be definite. However, a Poisson's ratio of 0.5 shows the feature of fluid, which cannot sustain shear stress. Therefore, the formation of shear band localization is expected to occur continuously throughout the material. In other words, shear band width approaches infinite.

To attain the absolute band width for a certain material, the internal length scale l must be determined in advance. Gradient models typically introduce internal length scales into their constitutive descriptions. Most of them attribute the internal length scale with the micro-structural size, the external loads and other material properties. For example, it was shown by Roscoe (1970), Mühlhaus and Vardoulakis (1987), that the thickness of the shear band is of several times of the mean grain diameter d_{50} for granular materials. In Al Hattamleh et al. (2004), it was further demonstrated that other factors, such as the external confining pressures and elastic properties, may also act as influential components to the length scale. However, the

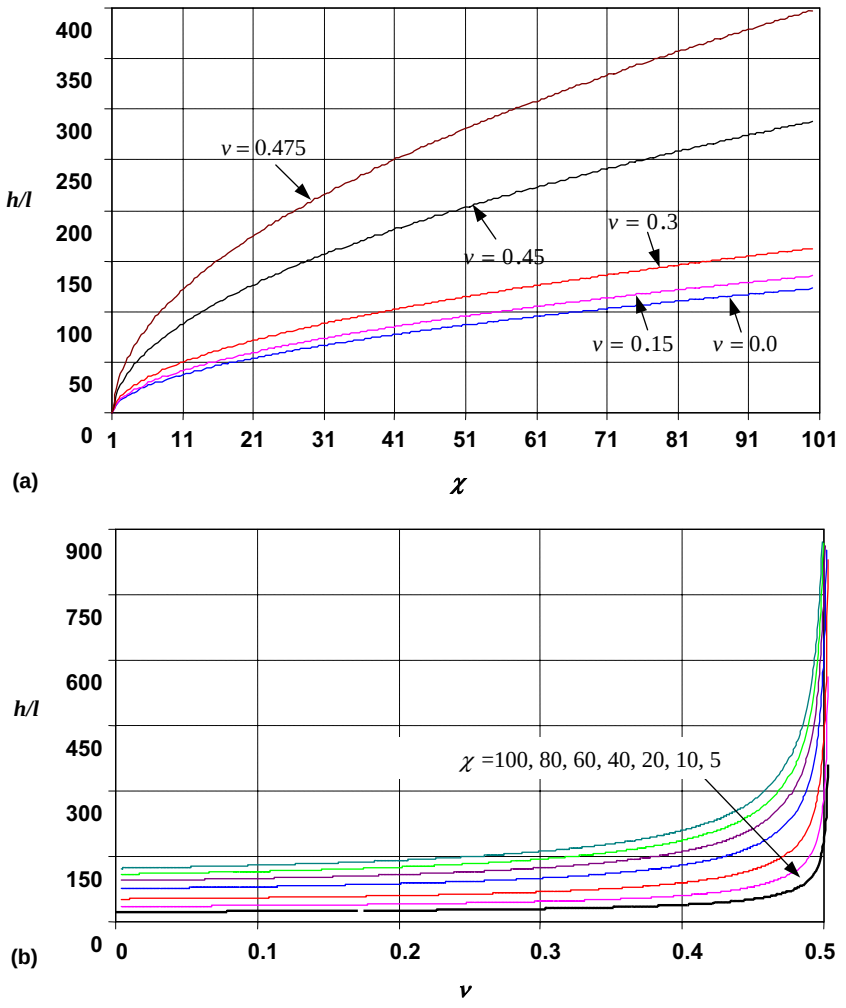

Fig. 3. Sensitivity of shear banding width to ν and χ. (a) χ versus h/l under different Poisson's ratio. (b) Poisson's ratio ν versus h/l under different χ.

internal length scale functions differently in different gradient models, so that there is no unified physical interpretation of l. In this paper, the internal length scale is regarded as a material constant that depends on the mean size of inhomogeneous microstructure in the material and may be experimentally determined, as has been stated in Zhou et al. (2002). For example, $l \approx 0.53$ mm for coal rock, $l \approx 0.47$ mm for sandstone and $l \approx 1.5$ mm for granite. For rock-like geomaterials, χ is reasonably ranged from 3.0 to 8.0 (see, e.g., Jaeger, 1979). If here κ_c is assumed to be $4\kappa_0$ so that $\chi = 4$ and ν is assumed to be 0.2, the corresponding shear band widths for coal rock, sandstone and granite are 11.96 mm, 11.6 mm and 33.84 mm, respectively. These results agree favorably with the experimental obtained data for these materials (Zhao, 2002). Typical band width has also been previously related with gradient coefficients by Aifantis (1984) and Zbib and Aifantis (1988), and was further calibrated by Panger et al. (1991) through experimental tension data of steel. They obtained a range of band width from 2.0 mm to 6.3 mm for a group of steel specimens. If these band widths are used to calibrate the length scale in our model and model parameters of $\chi = 2$ and $\nu = 0.28$

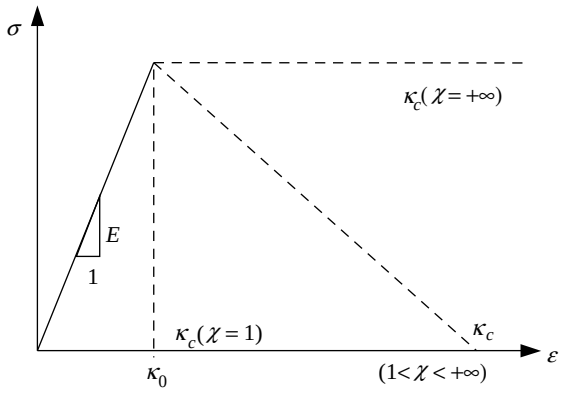

Fig. 4. Two extreme cases for the unixial stress–strain curve.

typical for steel are adopted, it is readily to obtain the internal length scale for the experimental steel ranges $0.15 \sim 0.47$ mm.

Note that size effects may also be addressed by the model in this paper. If the same problem of simple shear test is treated, this can be readily done by assuming the test specimen has a limited length of L instead of infinite. The same procedure for the solutions as presented in Section 3 may be repeated and consequently an additional specimen size scale is introduced into the final expression for all field variables. Based on this, the dependencies of shear band width, strains and strain gradients, as well as Cauchy stresses and higher-order stresses on this size scale may all be investigated. Furthermore, if the uniaxial softening law used in Fig. 1 is reformulated to express the peak strength in terms of other model parameters, the size effects of material strength may also be addressed.

4.2. Shear strain and shear strain gradient

As Eq. (58) indicates, the shear strain rate yields a cosine distribution within the band, but an exponential decay outside the band. A sensitivity study of the shear strain rate to χ and v is conducted and further verifies this point. Fig. 5 depicts the distribution of the shear strain rate under different values of χ. In the figure, the shear strain rate is normalized by $\dot{\sigma}^0_{21}/G$, and the distance to the band centre line is normalized by band width. As is shown, the shear strain rate exhibits a maximum value at the band centre and decreases towards the band boundary. A larger χ generally results in a higher peak shear strain rate at the band centre, while the curves outside the band are largely the same for all values of χ. Clearly, the shear strain rate is continuous across the boundary, which is in accordance with the characteristic of the second-order surface.

The curves in Fig. 5 are independent of the Poisson's ratio. This may also be observed from Eq. (58), where ξ and h (or y) appear in pairs and thus remove v in the final expression of the strain rate. This is a unique feature of the loading condition of the pure plane shear. For other cases with more complex loading conditions, such as biaxial or triaxial loading, the shear strain rate is generally dependent on Poisson's ratio.

The distribution of the shear strain in Aifantis (1987) and Zbib and Aifantis (1988), as well as that obtained by numerical simulation of one-dimensional bar by Chambon et al. (1998), exhibited a bell shape like, with the maximum strain at the centre line of the band and the applied shear strain (also the minimum value) at infinite. This is slightly different from the results obtained in this paper, as shown in Fig. 5.

It is also of interest to study the distribution of the strain gradients. Eq. (59) indicates that the rate of the shear strain gradient has a sine distribution within the band, but an exponential decay outside the band. Fig. 6a and b shows the normalized distribution of the shear strain gradient under different values of v

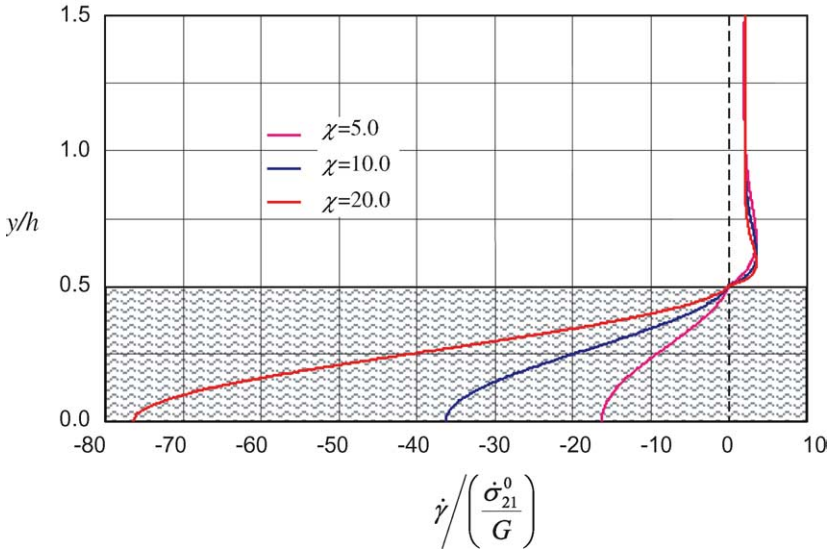

Fig. 5. Distribution of the normalized shear strain rate under different χ values.

and χ respectively. As can be seen in both figures, the normalized shear strain rate vanishes at the band centre. It reaches a maximum at around 0.26–0.27h and a minimum at 0.58–0.68h, and exponentially approaches zero at far field. As shown in Fig. 6a, a smaller Poisson's ratio generally leads to a higher peak within the band. When Poisson's ratio approaches 0.5, no obvious shear strain gradient is observed throughout the material. It is also observed that, under the same magnitude of $\chi = 5.0$, all curves for different values of v reach their maximum, minimum and zero at the same locations. Fig. 6b shows that, under the same value of $v = 0.15$, all curves for different values of χ start with a zero rate of the shear strain gradient at the band centre, reach a positive peak at around 0.26–0.27h. The larger χ is, the higher the peaks are. All curves passes through the band boundary into the non-localized area at the same point with a non-zero rate of the shear strain gradient.

However, the distribution of the strain gradient still differs from that of the strain in several ways. Firstly, the strain gradient does not vanish at the band boundary, whereas the strain does. Secondly, the location of the maximum strain gradient does not necessarily coincide with that of the maximum strain within the shear band. Thirdly, the Poisson's ratio has a significant influence on the distribution of the strain gradient, but a limited impact on the strain.

It is also noted that the strain gradient does not show an obvious jump across the band boundary, but it still satisfy the requirement of the second-order characteristic surface (Thomas, 1961).

4.3. Shear stress and higher-order stress

The distributions of the shear stress and the higher-order stress can be investigated using Eqs. (50), (51) and (58). In Fig. 7, the Cauchy shear stress rate $\dot{\sigma}_{21}$ and the higher-order stress rate $\dot{\tau}_{221}$ are normalized by $\dot{\sigma}^0_{21}$ and $l\dot{\sigma}^0_{21}$, respectively. Fig. 7a presents the distribution of the normalized shear stress rate under different χ values. As the shear strain rate, the Cauchy shear stress rate is independent of Poisson's ratio. The Cauchy shear stress rate exhibits a peak at the centre of the shear band, and then decreases to zero at the band boundary. The peak shear stress rates for different χ values are almost the same. Outside the shear band, the shear stress rate increases rapidly from zero to another peak value, and then decreases to the far-field

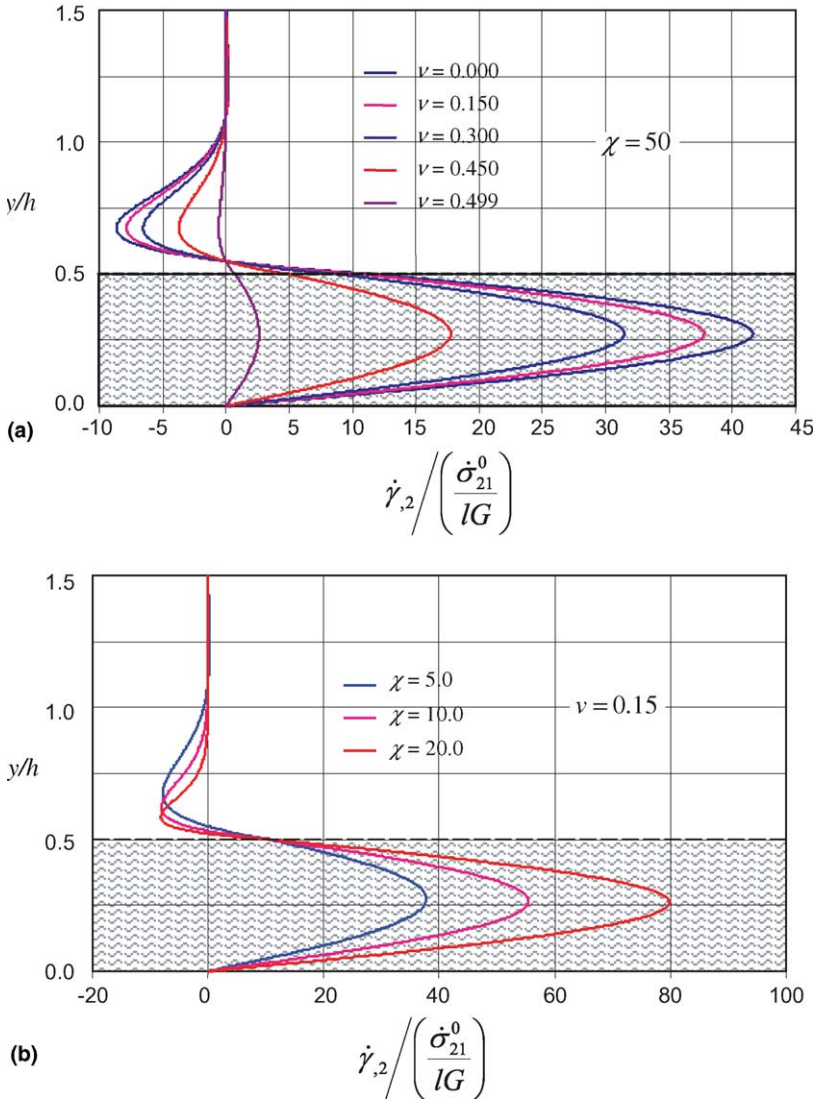

Fig. 6. Distribution of the normalized rate of the shear strain gradient. (a) Shear strain gradient rate under different ν values and $\chi = 5.0$; (b) shear strain gradient rate under different χ values and $\nu = 0.15$.

stress at infinity. In terms of the shear stress rate, the transition from the shear band to the non-localized zone is abrupt, even though still continuous. The larger χ is, the more dramatic this transition is.

Fig. 7b and c shows the distribution of the normalized higher-order stress rate under different ν and χ values, respectively. The general pattern of the higher-order stress rate within and outside the shear band is similar to that of the strain gradient rate (Fig. 6). Larger values of χ generally lead to higher peaks of the higher-order stress within the band, as shown in Fig. 7b. Comparing Figs. 6a and 7c, we observe that Poisson's ratio influences the strain gradient and the higher-order stress in a different way. Larger values of ν generally lead to smaller peaks of the strain gradient within the band, but higher peaks of the higher-order stress. It is also observed that the normalized higher-order stress rate at the centre of the shear band becomes extremely large when ν approaches 0.5.

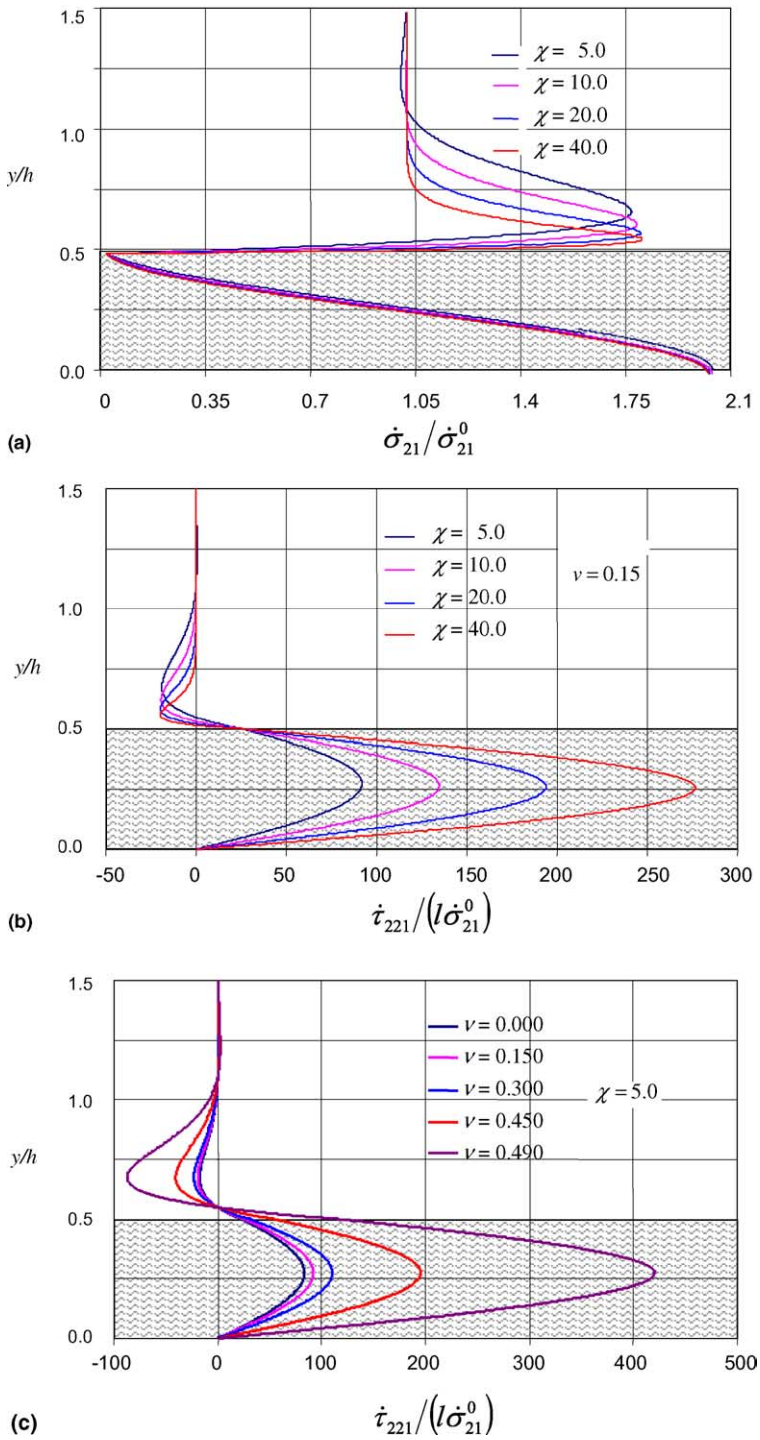

Fig. 7. Distribution of the normalized stress rates. (a) Shear stress rate under different χ values; (b) higher-order stress rate under different χ values and $\nu = 0.15$; (c) higher-order stress rate under different ν values and $\chi = 0.5$.

In a further comparative observation of Fig. 5–7 one may find, whatever the influence of either χ or Poisson's ratio may be, distributions for the strain, the strain gradient, the shear stress and the higher-order stress commonly exhibit dramatic changes around the shear band, while decay to be the prescribed magnitude at far field. This depicts an obvious boundary layer effect. In other words, the constitutive parameters used for the SGE damage model do affect the local deformation, strain gradients, stresses and higher-order stresses around the shear band, even though they have little effect on far-field physical quantities, such as the remotely applied stresses.

5. Conclusion

A strain-gradient-enhanced damage model is presented in this paper. The governing equations and the boundary conditions are obtained from the weak-form variational principle. The formulations presented in this paper are in accordance with those obtained by Toupin (1962) for the higher-order theory, Germain (1973) for a second gradient theory, and Aifantis (1987), Vardoulakis and Aifantis (1991) and Mühlhaus and Aifantis (1991) for the gradient plasticity theory. It should be noted that Aifantis (1987) is the first to obtain a shear band thickness within a softening plasticity model incorporating gradient effects, which substantially differentiates his work from the work of Toupin (1962) and Germain (1973), and also presents the basis for the subsequent work by Vardoulakis and Aifantis (1991) and Mühlhaus and Aifantis (1991).

Damage localization is thoroughly analyzed for the simple shear case using the isotropic form of the strain-gradient-enhanced damage model. Through a simple uniaxial stress–strain relation, the analytical solutions to the shear band localization are obtained. The obtained solutions satisfy the requirement of the second-order characteristic surface of Thomas (1961) and the condition of weak discontinuous bifurcation.

It is demonstrated the shear band width is proportionally related to the internal length scale and the proportionality is a function of Poisson's ratio v and a coefficient χ for the shape of the uniaxial stress–strain curve. In the specific case of plane simple shear test, external boundary conditions, such as far-field load or displacement restrictions, have no influence on this width. The strain and strain gradient exhibit a cosine and sine distribution within the band respectively, and both decay exponentially in the non-localized zone.

Numerical investigations of the analytical solutions for the simple shear test are carried out. Distributions of the shear strain, the shear strain gradient, the Cauchy shear stress and the higher-order shear stress show that they generally comply with the characteristic of the second-order discontinuous surface defined by Thomas (1961). Sensitivity studies of these distributions to χ and v are also conducted and compared.

The model and approach presented in this paper is also suitable to address the problem of size effects in materials. As has been pointed out in the paper, appropriate modifications of the boundary conditions in deriving the solutions to the simple shear problem will readily make the size effects accountable. Actually, the underlying theory of this model, the Fleck–Hutchinson's higher-order theory, was initially developed to describe size effects in microscopic experiments of materials. This model is thus essentially capable of addressing size effects problem in materials.

Acknowledgment

Part of this work was financially supported by National Science Foundation of China (NSFC through grant no. 50279016) and subsidized by the Special Funds for Major State Basic Research Projects (through grant no. 2002cb412708). Comments from the two anonymous reviewers were deeply appreciated. The first author is also grateful to Prof. Shouwen Yu of Tsinghua University for his helpful suggestions on this work.

References

Aifantis, E.C., 1984. On the microstructural origin of certain inelastic models. Trans. ASME J. Eng. Mater. Tech. 106, 326–330.

Aifantis, E.C., 1987. The physics of plastic deformation. Int. J. Plast. 3, 211–247.

Aifantis, E.C., 2001. Gradient plasticity. In: Lemaitre, J. (Ed.), Handbook of Materials Behavior Models. Academic Press, New York, pp. 291–307.

Aifantis, E.C., 2003. Update on a class of gradient theories. Mech. Mater. 35, 259–280.

Al Hattamleh, O., Muhunthan, B., Zbib, H.M., 2004. Gradient plasticity modelling of strain localization in granular materials. Int. J. Numer. Anal. Meth. Geomech. 28, 465–481.

Askes, H., Sluys, L.J., 2003. A classification of higher-order strain-gradient models in damage mechanics. Arch. Appl. Mech. 73, 448–465.

Chambon, R., Caillerie, D., El Hassan, N., 1998. One-dimensional localisation studied with a second grade model. Eur. J. Mech.—A/Solids 17 (4), 637–656.

Chambon, R., Caillerie, D., Matsuchima, T., 2001. Plastic continuum with microstructure, local second gradient theories for geomaterials: Localization studies. Int. J. Solids Struct. 38, 8503–8527.

De Borst, R., Mühlhaus, H.B., 1992. Gradient dependent plasticity: Formulation and algorithmic aspects. Int. J. Numer. Meth. Eng. 35, 521–539.

De Borst, R., Van der Giessen, E., 1998. Material Instabilities in Solids. John Wiley & Sons, Chichester.

Fleck, N.A., Hutchinson, J.W., 1993. A phenomenological theory for strain gradient effects in plasticity. J. Mech. Phys. Solids 41 (12), 1825–1857.

Fleck, N.A., Hutchinson, J.W., 1997. Strain gradient plasticity. In: Hutchinson, J.W., Wu, T.Y. (Eds.), Advances in Applied Mechanics, vol. 33. Academic Press, New York, pp. 295–361.

Fleck, N.A., Hutchinson, J.W., 2001. A reformulation of strain gradient plasticity. J. Mech. Phys. Solids 49, 2245–2271.

Gao, H., Huang, Y., Nix, W.D., Hutchinson, J.W., 1999. Mechanism-based strain gradient plasticity. I. Theory. J. Mech. Phys. Solids 47, 1239–1263.

Germain, P., 1973. The method of virtual power in continuum mechanics. Part 2: microstructure. SIAM J. Appl. Math. 25 (3), 556–575.

Gutkin, M.Y., Aifantis, E.C., 1999. Dislocations and disclinations in gradient elasticity. Phys. Status Solidi 214B, 245–284.

Hadamad, J., 1903. Lecons sur la propagation des ondes et les équations de l'hydrodynamique. Librarie Scientifique. A. Hermann, Paris.

Hill, R., 1958. A general theory of uniqueness and stability in elastic–plastic solids. J. Mech. Phys. Solids 6, 236–249.

Jaeger, C., 1979. Rock Mechanics and Engineering. Cambridge University Press, New York.

Koiter, W., 1964. Couple-stress in the theory of elasticity. Mech. Ser. B 2, 17–44.

Konstantinidis, A., Aifantis, E.C., 2002. Recent developments in gradient plasticity. Part I: formulation and size effects. J. Eng. Mater. Tech. 124, 358–364.

Kuhl, E., Ramm, E., 2000. Simulation of strain localization with gradient with gradient enhanced damage models. Comput. Mater. Sci. 16, 176–185.

Mindlin, R.D., 1964. Micro-structure in linear elasticity. Arch. Rat. Mech. Anal. 16, 51–78.

Mindlin, R.D., 1965. Second gradient of strain and surface tension in linear elasticity. Int. J. Solids Struct. 28, 845–857.

Mühlhaus, H.B., Aifantis, E.C., 1991. A variational principle for gradient plasticity. Int. J. Solids Struct. 28, 845–857.

Mühlhaus, H.B., Vardoulakis, I., 1987. The thickness of shear bands in granular materials. Géotechnique 37, 217–283.

Ottosen, N.E., Runesson, K., 1991. Properties of discontinuous bifurcation solutions in elasto-plasticity. Int. J. Solids Struct. 27 (4), 401–421.

Panger, G.L., Ding, J.L., Zbib, H.M., Aifantis, E.C., 1991. Measurement of shear band characteristics in low carbon steel using photoelasticity. Scr. Metall. Mater. 25, 2103–2108.

Peerlings, R.H.J., de Borst, R., Brekelmans, W.A.M., Vree, J.H.P., 1996. Gradient enhanced damage for quasi-brittle materials. Int. J. Numer. Meth. Eng. 39, 3391–3404.

Pietruszczak, S.T., Mroz, Z., 1981. Finite element analysis of deformation of strain softening materials. Int. J. Numer. Meth. Eng. 17, 327–334.

Roscoe, K.H., 1970. The influence of strain in soil mechanics, 10th Rankine lecture. Géotechnique 20(2), 129–170.

Rudnicki, J.W., 1977. The inception of faulting in a rockmass with a weakened zone. J. Geophys. Res. 82, 844–854.

Rudnicki, J.W., Rice, J.R., 1975. Conditions for the localization of deformation in pressure-sensitive dilatant materials. J. Mech. Phys. Solids 23, 371–395.

Shi, M.X., Huang, Y., Hwang, K.C., 2000. Plastic flow localization in mechanism-based strain gradient plasticity. Int. J. Mech. Sci. 42, 2115–2131.

Shu, J.Y., Fleck, N.A., 1999. Strain gradient crystal plasticity: size-dependent deformation of bicrystals. J. Mech. Phys. Solids 47, 297–324.

Thomas, T., 1961. Plastic Flow and Fracture in Solids. Academic Press, New York.
Toupin, R.A., 1962. Elastic materials with couple stresses. Arch. Ration. Mech. Anal. 11, 385–414.
Triantafyllidis, N., Aifantis, E.C., 1986. A gradient approach to localization of deformation. I. Hyperelastic materials. J. Elast. 16, 225–238.
Tsagrakis, I., Aifantis, E.C., 2002. Recent developments in gradient plasticity. Part I: formulation and size effects. J. Eng. Mater. Tech. 124, 352–357.
Tsagrakis, I., Aifantis, E.C., 2003a. Element-free Galerkin implementation of gradient plasticity. Part I: formulation and application to 1D strain localization. J. Mech. Beh. Mater. 14, 199–231.
Tsagrakis, I., Aifantis, E.C., 2003b. Element-free Galerkin implementation of gradient plasticity. Part II: application to 2D strain localization and size effects. J. Mech. Beh. Mater. 14, 233–270.
Tsagrakis, I., Konstantinidis, A., Aifantis, E.C., 2003. Strain gradient and wavelet interpretation of size effects in yield and strength. Mech. Mater. 35, 733–745.
Vardoulakis, I., Aifantis, E.C., 1991. A gradient flow theory of plasticity for granular materials. Acta Mech. 87, 197–217.
Zbib, H.M., Aifantis, E.C., 1988. On the structure and width of shear bands. Scr. Met. 22, 703–708.
Zbib, H.M., Aifantis, E.C., 1989. A gradient-dependent flow theory of plasticity: application to metal and soil instabilities. Appl. Mech. Rev. 42, 295–304.
Zbib, H.M., Aifantis, E.C., 1992. On the gradient-dependent theory of plasticity and shear banding. Acta Mech. 92, 209–225.
Zhao, J.D., 2002. Localization failure study of geomaterials by strain-gradient-enhanced damage models. Ph.D. dissertation. Tsinghua University, Beijing, China.
Zhou, W.Y., Zhao, J.D., Liu, Y.G., Yang, Q., 2002. Simulation of localization failure with strain-gradient-enhanced damage mechanics. Int. J. Numer. Anal. Meth. Geomech. 26, 793–813.